



HAL
open science

Crack in the frictional interface as a solitary wave

Oleg Braun, Michel Peyrard

► **To cite this version:**

Oleg Braun, Michel Peyrard. Crack in the frictional interface as a solitary wave. *Physical Review E: Statistical, Nonlinear, and Soft Matter Physics*, 2012, 85, pp.026111-1-10. 10.1103/PhysRevE.85.026111 . ensl-00673957

HAL Id: ensl-00673957

<https://ens-lyon.hal.science/ensl-00673957>

Submitted on 24 Feb 2012

HAL is a multi-disciplinary open access archive for the deposit and dissemination of scientific research documents, whether they are published or not. The documents may come from teaching and research institutions in France or abroad, or from public or private research centers.

L'archive ouverte pluridisciplinaire **HAL**, est destinée au dépôt et à la diffusion de documents scientifiques de niveau recherche, publiés ou non, émanant des établissements d'enseignement et de recherche français ou étrangers, des laboratoires publics ou privés.

Crack in the frictional interface as a solitary wave

O. M. Braun*

Institute of Physics, National Academy of Sciences of Ukraine, 46 Science Avenue, UA-03028 Kiev, Ukraine

M. Peyrard†

Laboratoire de Physique de l'Ecole Normale Supérieure de Lyon, 46 Allée d'Italie, FR-69364 Lyon Cédex 07, France

(Received 28 October 2011; revised manuscript received 18 January 2012; published 21 February 2012)

We introduce and investigate a multiscale model for the propagation of rupture fronts in friction. Taking advantage of the correlation length for the motion of individual contacts in elastic theory, we introduce collective contacts which can be characterized by a master equation approach. The problem of the dynamics of a chain of those effective contacts under stress is studied. We show that it can be reduced to an analog of the Frenkel-Kontorova model. In some limits this allows us to derive analytical solutions for kinks describing the rupture fronts. Numerical simulations are used to study more complex cases.

DOI: [10.1103/PhysRevE.85.026111](https://doi.org/10.1103/PhysRevE.85.026111)

PACS number(s): 81.40.Pq, 46.55.+d

I. INTRODUCTION

Friction between two solids results from multiple contacts which break under stress and form again elsewhere later. Although they are far from being fully understood, the basic laws of these phenomena can be discussed in terms of the statistics of these local contacts, which can be viewed at different scales, from the atomic contacts involved in atomic force microscopy (AFM) studies to micro- or millimeter asperities between two macroscopic solids. At macro- or mesoscales, the modeling of friction can be done by describing the evolution of a distribution that characterizes the stress of the individual contacts, in terms of a master equation (ME) that governs the space-time evolution of this distribution [1,2]. However, the *onset* of the frictional slip is difficult to describe because the overall motion is preceded by local precursors. The motion starts at weak points, causing *localized fractures* at the interface between the solids in contacts. Experiments point out the importance of three different types of detachment fronts: (i) Rayleigh (surface sound) fronts, (ii) slow detachment fronts, and (iii) fast fronts [3]. These fronts propagate with different speeds, and appear to play a role in the onset of sliding at the scale of the laboratory experiments as well as at the scale of faults in earthquakes.

The idea that local ruptures are important for friction is not new. For instance, the “waves of detachment” observed by Schallamach [4] correspond to this phenomenon. However, the physics behind the propagation of the different modes of friction fronts is not yet understood.

In this work we propose a multiscale model to describe the fronts at the onset of friction, which describes the breaking and formation of contacts which may themselves result from many events at a smaller scale. The statistical description of those small-scale events defines the properties of the *effective contacts* which enter in the description of the front observed experimentally. Section II introduces this model and shows how it can be reduced to a standard soliton-bearing model, a

modified version of the Frenkel-Kontorova (FK) model. Using a continuum limit approximation, Sec. III derives analytical results which are tested by numerical simulations in Sec. IV. Section V discusses the results and possible extensions of this work.

II. THE FK-ME MODEL

A. A decomposition of the physical problem of friction

As schematically shown in Fig. 1(a), when two macroscopic objects are brought into contact, they only touch each other at a discrete set of points, labeled by an index i , while large parts of the interface are actually separated by a distance which is well above the range of the interatomic interactions. The mechanics of the interface must take into account two phenomena: (1) the properties of the individual contacts themselves, which are stretched by an amount x_i when a shear stress is applied to the interface, and (2) the deformation of the underlying substrate, which may deform to redistribute the shear stresses σ_i among the individual contacts.

Elastic theory introduces a characteristic size λ_c for which the interface may be considered as rigid [5,6]. The calculation of λ_c requires the solution of the three-dimensional elastic problem, but this concept can be understood from simple qualitative arguments. When an asperity, characterized by an elastic constant k_i , is displaced by δx , the resulting local stress is $\sigma \approx k_i \delta x / a^2$, where a^2 is the area per contact. It induces a strain $\epsilon = \sigma / E$ of the interface, where E is the Young modulus of the material. For another asperity at distance ℓ this induces a displacement $\delta \ell \approx \epsilon \ell = \ell(k_i \delta x) / (a^2 E)$. This displacement, which is small as long as ℓ is small enough, can be neglected up to $\ell = \lambda_c$ for which $\delta \ell \approx \delta x$, i.e., the distortion of the interface is of the order of the stretching of the asperities. This gives $\lambda_c \approx a^2 E / k_i$. For a material such as steel, λ_c is in the range 10–100 μm , a value that is large compared to the typical distance between asperities; however it is important to notice that the actual value of λ_c can vary widely, depending on the geometry of the interface and conditions of an experiment. To get an estimate, let us consider a contact of cylindrical shape of radius r and height h . The elastic constant of this flexible “rod” is [7] $k_i = 3EI/h^3$, where $I = \pi r^4/4$ is an effective

*obraun.gm@gmail.com; <http://www.iop.kiev.ua/> obraun

†michel.peyrard@ens-lyon.fr

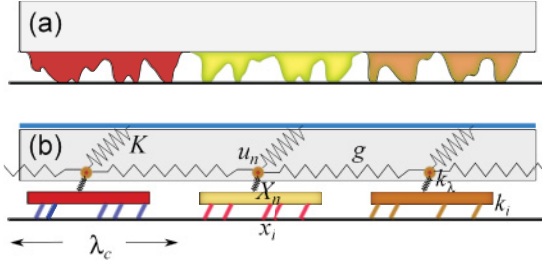


FIG. 1. (Color online) Schematic view explaining the decomposition of the friction problem into elements that are studied separately. (a) Contact of a rough interface with a flat substrate. We consider the bulk material (rectangle) and the interfacial rough layer, which has many asperities in contact with the substrate. (b) The reduced model. Asperities are correlated over a length λ_c and form a “ λ contact” composed of asperities, having elastic constants k_i , and a piece of material, between the asperities and the bottom of the bulk volume, having an elasticity k_λ . The n th λ contact is attached to the bulk material at position u_n . The bulk material is described by an elastic constant g that corresponds to its deformation along the interface, and the elastic constant K , which is associated to its shear deformation when its top surface is subjected to some shear stress.

moment of inertia of a section. We get

$$\lambda_c = \frac{4}{3\pi} \frac{a^2}{r} \left(\frac{h}{r}\right)^3. \quad (1)$$

Interestingly the result *only depends on the geometry* of the interface, and not on the nature of the material, stiff or soft. This is because the stiffness of the material enters both in the rigidity of a contact and in the rigidity of the interface. But, for this geometry, owing to the third power of the h/r term, λ_c can vary widely, surfaces with a deeper corrugation giving a larger λ_c . Things would become even more complex if one considers lubricated friction, for which the elastic properties of the contact can become different from that of the bulk, or if one takes into account the fact that the geometry of the contacts (for instance the ratio h/r) depends on pressure.

As shown in Fig. 1(b), if the substrate can be considered as rigid in a region of size λ_c , this allows us to split the friction problem in two parts. At the smallest scale one can study the collective behavior of a set of contacts attached to a “rigid body” of typical size λ_c , which is itself related to the bulk by an elastic spring of rigidity k_λ describing the elastic response of the part of material that is between the asperities and the bulk. We henceforth call λ contact this set of microscopic contacts. At a larger scale the elastic deformation of the sliding block cannot be ignored. The λ contacts are elastically coupled through the deformation of the bulk.

Therefore the friction problem can be approached in two steps: (a) study the collective behavior of the individual contacts to determine the effective properties of the λ contact, such as its breaking threshold, or the relation between its stretching and the shear stress applied between the bulk and the underlying substrate; and (b) study the collective behavior of the λ contacts taking into account the elasticity of the sliding block. This approach can be considered as a variant of the usual finite element method of elasticity to the problem of friction. The λ contacts are the finite elements that have to be

connected to each other, and to another element which is the elastic bulk, to describe the complete system.

B. Characteristics of a λ contact

A λ contact is an effective contact which involves many individual contacts. Its properties are therefore determined by the statistics of the individual events occurring at the level of each of those individual contacts, i.e., the sequence of breakings and reattachments and by the elastic properties of the material forming the λ contact, schematized by a particular color in Fig. 1(a). As shown earlier [1,2] the collective properties of many contacts connected to a rigid substrate can be described in terms of a ME. We denote by X_n the displacement of the rigid block corresponding to the center of the n th λ contact. In this section we shall drop the index n as we are considering a given λ contact. Let us denote by x_i the stretching of the local contacts i which belong to the λ contact. The statistical ME approach does not intend to study the individual x_i but instead to describe the evolution of the distribution of stretchings x_i as a function of the position X of the rigid block. We denote by $Q(x, X)$ this normalized distribution. The friction force at the level of the λ contact is the sum of the elastic forces at all the local asperities, i.e.,

$$F(X) = N_\lambda \langle k_i \rangle \int_{-\infty}^{+\infty} dx x Q(x; X), \quad (2)$$

where N_λ is the average number of individual contacts forming a λ contact and k_i the elastic constant of an individual contact. Writing the balance between the contacts that break when the rigid block is moved by ΔX and the contacts that attach again after breaking, leads to an integrodifferential equation for $Q(x; X)$ [1,2],

$$\begin{aligned} \frac{\partial Q(x; X)}{\partial x} + \frac{\partial Q(x; X)}{\partial X} + P(x)Q(x; X) \\ = R(x) \int_{-\infty}^{+\infty} d\xi P(\xi)Q(\xi; X), \end{aligned} \quad (3)$$

where $P(x)\Delta X$ is the fraction of contacts that break when the position of the block changes from X to $X + \Delta X$. It is related to the statistical properties of the individual contacts, which are characterized by a threshold x_c , which is the stretching above which they break. If $P_c(x_c)$ is the normalized probability distribution at which individual contacts break, one has [1,2]

$$P(x) = P_c(x) \int_x^\infty d\xi P_c(\xi). \quad (4)$$

$R(x)$ is the distribution of the stretching of the individual contacts when they attach again after breaking. In the simplest case one can assume that it is simply the Dirac delta distribution $R(x) = \delta(x)$.

In the simplified view of Fig. 1, the rigid block formed by a set of individual contacts grouped into a λ contact is connected to the bulk by an elastic spring k_λ , which represents the average flexibility of the material which is between the asperities of the λ contact and the bottom surface of the bulk. We denote by u the point of the bulk to which the λ contact is attached, i.e., the elastic energy associated to the overall deformation of the λ contact is $\frac{1}{2}k_\lambda(u - X)^2$. If we neglect dynamics within a λ contact, u and X evolve together, up to a constant, so

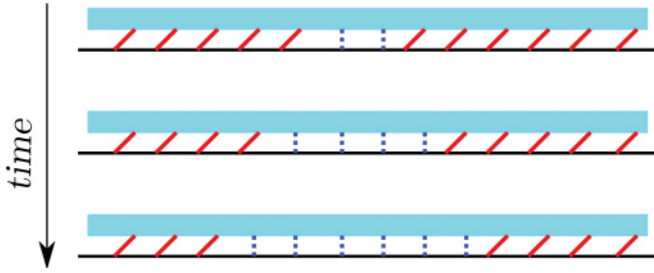


FIG. 2. (Color online) Schematic picture showing the propagation of the friction fronts generated at weak points in the center of the system. The thick (red) lines represent λ contacts which have been stretched by the shear. The (blue) dotted lines represent λ contacts which have relaxed by sliding. As time grows the relaxed region extends and its boundaries make two kinks separating domains where the λ contacts are in different states.

that we can express the force exerted by the λ contact on the bulk as $F(u)$, where the function F is determined by Eq. (2). Qualitatively we expect $F(u)$ to be a growing function of u , up to a threshold u_c for which the λ contact reaches a local elastic instability and starts to slide. This releases the stress on the asperities and the effective contacts form again. The friction force on a λ contact is therefore periodic because it results from a stick slip at the scale of the λ contact. The exact function $F(u)$, which may be complex, has to be derived from the ME approach and the properties of the individual contacts. An example is shown in Fig. 3 below and studied in Sec. IV.

C. The model of the interface

Let us consider a one-dimensional view of the interface in the direction of the applied stress, i.e., a chain of λ contacts. They are coupled by the elasticity of the bulk. We denote by g the corresponding elastic constant [Fig. 1(b)]. The top surface of the block is driven at a velocity v_d . This applies a shear stress to the block, which is transmitted to each λ contact by the shear elasticity of the block, described by the harmonic coupling constant K . And, as discussed above, the λ contact n is coupled “frictionally” with the bottom substrate by a nonlinear force $F(u_n)$. The equation of motion of the chain of λ contacts is therefore

$$m\ddot{u}_n + m\eta\dot{u}_n - g(u_{n+1} + u_{n-1} - 2u_n) + F(u_n) + Ku_n = f, \quad (5)$$

where m is an effective mass and η is a friction coefficient that describes all mechanisms for energy transfer away from the interface. The driving force f is chosen to be

$$f(t) = K(v_d t + x_{\text{ini}}) \quad (6)$$

(x_{ini} will only be used in the numerical simulations; it reduces the simulation time by initiating the calculation with a nonzero force). In Eq. (6) all λ contacts are assumed to be the same. The surface of a solid is of course never perfectly homogeneous, but, as the λ contacts are effective contacts involving many individual asperities, in comparison with individual asperities, the width of their distribution of breaking thresholds is reduced by a factor $1/\sqrt{N_\lambda}$, which makes this approximation reasonable.

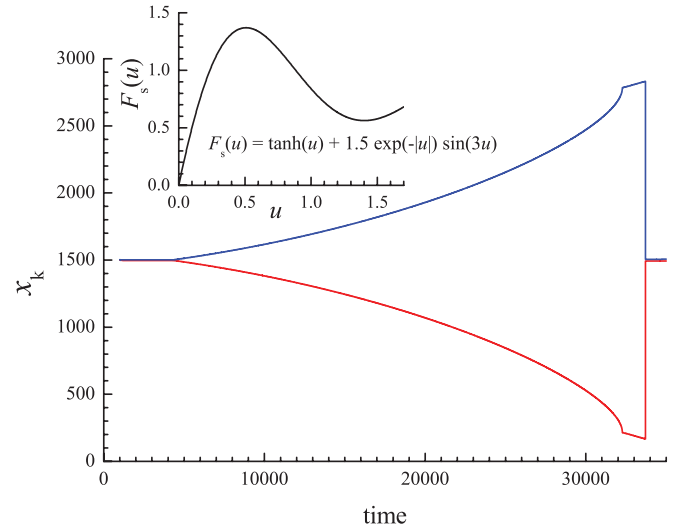


FIG. 3. (Color online) Typical evolution of the chain of contacts. The nearest neighboring contacts interact elastically with the constant $g = 5$. The interaction with the substrate is modeled by the function (see inset) $F(u) = k[\tanh(u) + 1.5e^{-|u|} \sin(3u)]$ for $0 \leq u < u_c = 1$ and periodically prolonged for other values of u ($k = 1$). All contacts are driven through the springs of the elastic constant $K = 0.07$, their ends moving with the velocity $v_d = 10^{-4}$. The motion is overdamped ($m = 1$, $\eta = 100$). To initiate the breaking, two central contacts interact with the substrate with smaller values of the elastic constant, $k' = 0.5$ (when the kinks begin to move, the central contacts restore their values to $k = 1$; to speed up the simulation, we used $x_{\text{ini}} = 16.9$). The curves show the kinks centers (defined as places where the atomic velocity is maximal). The chain has length $N = 3000$ with periodic boundary condition; when the kinks reach the ends and collide, they annihilate.

As discussed above, in this multiscale approach the substrate force $F(u)$ has to be derived from the solution of the ME approach applied to a λ contact. The general case can only be studied numerically (see Sec. IV below). A typical evolution of the chain is shown in Figs. 2–4. In these calculations the friction front is initiated by starting with two weaker λ contacts at the center of the system. As soon as the front is created the parameters at those sites are restored to their normal values. As schematized in Fig. 2 the dynamics starts by the relaxation of these two λ contacts which slide. This causes an extra stress on the neighboring contacts, which tend to slide too, and then the sliding events propagate as a kink and an antikink that move away from each other, extending the initial relaxed domain. Our purpose in this work is to describe the type of collective phenomena that occur when those fronts propagate, to provide an analytical understanding in some simplified cases, and to characterize the properties of the fronts and their relations with the experiments observing rupture fronts in friction.

Let us first consider a simplified case, when $F(u)$ can be approximated by the sawtooth shape, i.e., it is introduced as

$$F(u) = ku \quad \text{for } 0 \leq u < u_c \quad (7)$$

and periodically prolonged for other values of u . In the calculations, the shear force f depends on time, which allows us to observe the properties of the fronts subjected to different forces in a single simulation. However, the variation

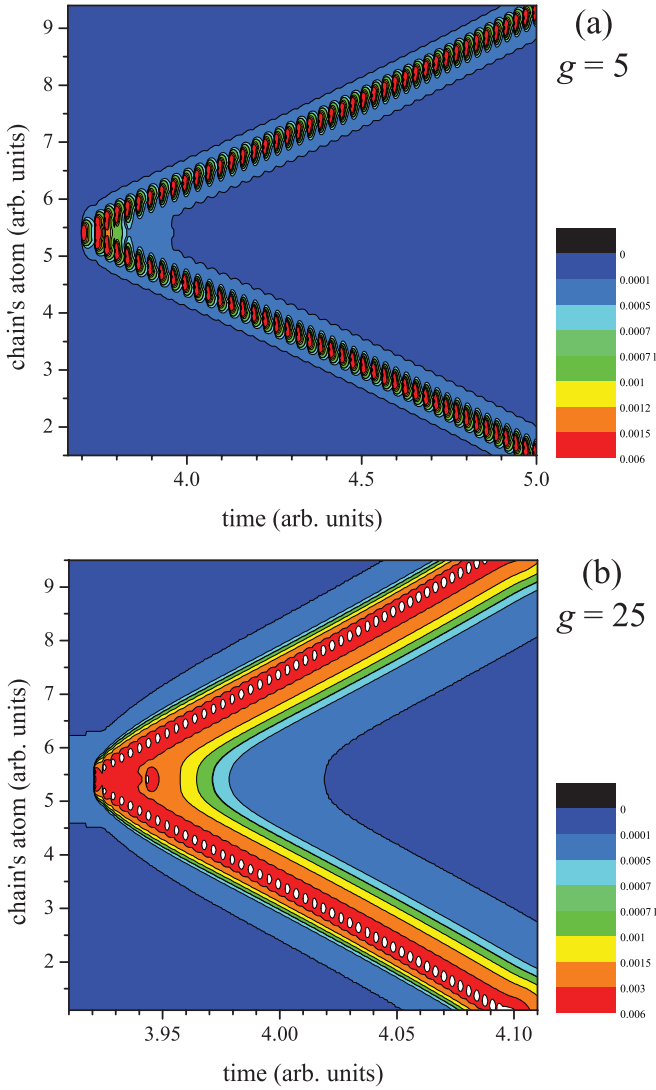


FIG. 4. (Color online) Typical evolution of the chain of contacts. The interaction with the substrate is modeled by the function as described by the function $F(u)$ defined in the caption of Fig. 3. Color map of atomic velocities for two values of the interaction between the contacts: (a) $g = 5$ and (b) $g = 25$; other parameters as in Fig. 3.

is sufficiently slow to allow us to follow the kink propagation long enough before f has changed in an appreciable way (adiabatic approximation). This is correct if the change of the driving force $\Delta f = K v_d \Delta t$ during kink motion through the chain, $\Delta t = L/v$ (L is the chain length and v is kink velocity), is much lower than ku_c , or

$$K/k \ll (v/v_d)(u_c/L). \quad (8)$$

Let us define the function

$$\mathcal{F}(u) = F(u) + Ku - f. \quad (9)$$

The ground state of the chain is degenerate and determined by the equation $\mathcal{F}(u) = 0$. A graphical solution of this equation is plotted in Fig. 5, where we also show the “effective potential” $V_{\text{eff}}(u) = \int du \mathcal{F}(u)$. Note that the ground-state solutions are stable, because $d\mathcal{F}(u)/du = k + K > 0$.

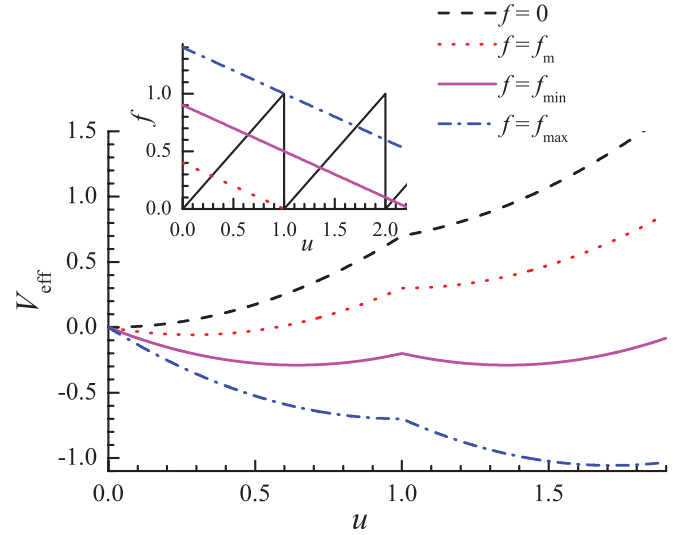


FIG. 5. (Color online) The effective FK-like “potential” $V_{\text{eff}}(u) = \int du \mathcal{F}(u)$ for $u_c = 1$, $k = 1$, and $K = 0.4$ and different values of the driving force: $f = 0$ (no driving), $f = f_m = Ku_c$ (when the second local minimum appears), $f = f_{\text{min}} = (\frac{1}{2}k + K)u_c$ (the two local minima are characterized by the same energy), and $f = f_{\text{max}} = (k + K)u_c$ (the left minimum disappears). Inset shows graphical solution of the equation $\mathcal{F}(u) = 0$, or $F(u) = f - Ku$.

The case of a single kink is obtained if we let the right-hand side ($n \rightarrow \infty$) of the chain be unrelaxed, $ku_R + Ku_R = f$, or

$$u_R = f/(k + K), \quad (10)$$

while the left-hand side ($n \rightarrow -\infty$) already undergone relaxation, $k(u_L - u_c) + Ku_L = f$, or

$$u_L = (f + ku_c)/(k + K), \quad (11)$$

as shown in Fig. 2. The kink interpolates between these two states, which correspond to different minima of the effective potential.

As a result this model appears as a variant of the standard Frenkel-Kontorova model [8]. We call it henceforth the FK-ME model as a reminder of its double connection with the Frenkel-Kontorova model and the master equation approach. It is described by Eqs. (5)–(7) with the boundary conditions given by Eqs. (10) and (11).

III. CONTINUUM-LIMIT APPROXIMATION

In a first approach, let the system be overdamped ($\ddot{u} = 0$); later on we shall remove this restriction. The continuum approximation is a standard method to derive an approximate solution of the Frenkel-Kontorova model. In this approximation the discrete index n is replaced by the continuous space variable x , $n \rightarrow x = na$ where a is the spacing between the λ contacts. The equation of motion takes the form

$$m\eta u_t - a^2 g u_{xx} + \mathcal{F}(u) = 0, \quad \mathcal{F}(u)|_{x \rightarrow \pm\infty} = 0, \quad (12)$$

where $u_t = \partial u / \partial t$ and $u_{xx} = \partial^2 u / \partial x^2$. We look for a solution in the form of a wave of stationary profile (the solitary wave in

the continuum limit of the FK model), $u(x, t) = u(x - vt)$, so that $u_t = -vu'$ and $u_{xx} = u''$. In this case Eq. (12) becomes

$$m\eta v u' + a^2 g u'' = \mathcal{F}(u). \quad (13)$$

Introducing dimensionless variables $w = u/u_c$ and $x = by$ with a characteristic distance $b = ga^2/(m\eta v)$ so that $d/dx = b^{-1}d/dy$, we obtain

$$w_y + w_{yy} = G(w), \quad (14)$$

where the indices designate first and second derivatives with respect to y ,

$$G(w) = \frac{ga^2}{(m\eta v)^2 u_c} \mathcal{F}(u_c w), \quad (15)$$

and the following boundary conditions are to be imposed ($w_{L,R} = u_{L,R}/u_c$):

$$y \rightarrow -\infty: \quad w \rightarrow w_L, \quad G \rightarrow 0, \quad (16)$$

$$y \rightarrow +\infty: \quad w \rightarrow w_R, \quad G \rightarrow 0. \quad (17)$$

Notice that

$$w_L = w_R + k/(k + K) \quad (18)$$

and

$$w_c = 1. \quad (19)$$

A standard method to solve an equation such as Eq. (14) consists in introducing the function $p(w) = w_y$; then

$$w_{yy} = \frac{d}{dy} w_y = \frac{d}{dy} p(w) = \frac{dp}{dw} \frac{dw}{dy} = p \frac{dp}{dw},$$

and Eq. (14) reduces to $p(dp/dw) + p = G(w)$, or

$$\frac{dp(w)}{dw} = -1 + \frac{G(w)}{p(w)}, \quad (20)$$

with the boundary conditions

$$p(w_{L,R}) = 0 \quad \text{and} \quad G(w_{L,R}) = 0. \quad (21)$$

Using linear expansions near the boundaries,

$$G(w) = (w - w_{L,R})A, \quad (22)$$

where

$$A \equiv \left. \frac{dG(w)}{dw} \right|_{w=w_{L,R}} = \frac{ga^2(k + K)}{(m\eta v)^2} \quad (23)$$

and

$$p(w) = \left. \frac{dp(w)}{dw} \right|_{w=w_{L,R}} (w - w_{L,R}), \quad (24)$$

we find that

$$\left. \frac{dp}{dw} \right|_R = -\frac{1}{2}(1 + \sqrt{1 + 4A}) < 0 \quad (25)$$

and

$$\left. \frac{dp}{dw} \right|_L = \frac{1}{2}(\sqrt{1 + 4A} - 1) > 0. \quad (26)$$

A solution of Eq. (20) with these boundary conditions only exists for a certain value of the kink velocity v ; this finally determines the dependence $v(f)$.

For the sawtooth shape of $F(u)$, Eq. (7), the solution has the triangular shape: for $w_R \leq w \leq w_c$,

$$p(w) = p_R(w) = -\frac{1}{2}(1 + \sqrt{1 + 4A})(w - w_R), \quad (27)$$

while for $w_c \leq w \leq w_L$,

$$p(w) = p_L(w) = -\frac{1}{2}(\sqrt{1 + 4A} - 1)(w_L - w). \quad (28)$$

The continuity condition $p_R(w_c) = p_L(w_c)$ gives us an equation for v :

$$\sqrt{1 + 4A} = \frac{q + 1}{q - 1}, \quad (29)$$

where

$$q = \frac{w_L - w_c}{w_c - w_R} > 1. \quad (30)$$

It is convenient to introduce the parameter $k_* = f/u_c$. Then we have

$$q = \frac{k_* - K}{k + K - k_*} = \frac{1}{\beta - 1}, \quad (31)$$

where

$$\beta = k/(k_* - K) = 1 + 1/q, \quad (32)$$

and the continuity equation (the equation for v) reduces to

$$(m\eta v)^2 = ga^2(k + K) \frac{(2 - \beta)^2}{\beta - 1}. \quad (33)$$

For the kink moving to the right with a velocity $v \geq 0$, the following inequality must be satisfied:

$$w_R < w_c < w_L - \frac{1}{2}(w_L - w_R), \quad (34)$$

which is equivalent to

$$\frac{k_*}{k + K} < 1 < \frac{\frac{1}{2}k + k_*}{k + K},$$

or $k + K > k_* > \frac{1}{2}k + K$, $\infty > q > 1$ or $1 < \beta < 2$.

The limit $\beta = 2$, or $k_* = \frac{1}{2}k + K$, corresponds to zero kink velocity, $v = 0$, associated to the Griffith threshold for fractures, i.e., the minimal force which supports the kink motion:

$$f_{\min} = \left(\frac{1}{2}k + K\right)u_c. \quad (35)$$

The maximal force, for which a kink may exist, is defined by the limit $\beta = 1$, or $k_* = k + K$:

$$f_{\max} = (k + K)u_c. \quad (36)$$

At higher forces, the barriers of $\mathcal{F}(u)$ and the stationary ground states disappear, and the whole chain of λ contacts is in a sliding state. This is the case when the limit of the static friction has been exceeded. For a smooth function $F(u)$ instead of the sawtooth shape used to get an analytical solution, this upper limit is lowered (see Sec. IV below).

From Eq. (33) we can find the kink velocity as a function of the driving force. At low velocities

$$v \approx (f - f_{\min})/m_k \eta, \quad (37)$$

where we introduced the effective kink mass

$$m_k = m \frac{4a}{u_c} \sqrt{\frac{g}{k} \left(1 + \frac{K}{k}\right)}, \quad (38)$$

while at $f \rightarrow f_{\max}$ the velocity tends to infinity,

$$m\eta v \approx \sqrt{\frac{gk(k+K)a^2 u_c}{(f_{\max} - f)}}. \quad (39)$$

The latter limit should be corrected by taking into account inertia effects. If we are no longer in the overdamped regime, the term $m\ddot{u}$ in Eq. (5) gives $mv^2 u''$ for the solitary-wave solution, so it can be incorporated if we substitute in the above equations $g \rightarrow g_{\text{eff}} = g(1 - v^2/c_0^2)$, where $c_0 = \sqrt{ga^2/m}$ is the sound speed along the chain. This is the well-known “relativistic” narrowing of kinks in Lorentz-invariant soliton equations. The high-velocity limit now takes the form

$$v \approx c_0 \sqrt{1 + \frac{m\eta^2(f_{\max} - f)}{k(k+K)u_c}}. \quad (40)$$

Above we have assumed that broken (detached) contacts immediately reappear, i.e., are immediately bound again to the substrate after relaxation. This is assumed in the choice of the sawtooth expression for $F(u)$. The detachment-attachment events in our model are an analog of the opening-closing of the crack in fracture mechanics. In a more general model we have to take into consideration the aging of contacts, i.e., a change of their parameters with time of contact. In the simplest approximation the aging may be included by assuming that, after they form again, the contacts keep a negligible friction force $F(u) \approx 0$ for some delay τ , and then recover the standard friction force. During τ , which is a new parameter of the model, the contact moves for a distance

$$l = v\tau, \quad (41)$$

and over this length the substrate force is kept to zero so that the substrate force is now given by Eq. (7), $F(u) = ku$ for $0 \leq u < u_c$, and $F(u) = 0$ for $u_c \leq u < u_c + l$. The new function $F(u)$ is periodic with the period $u_d = u_c + l$. Because the substrate force depends on the kink velocity v through Eq. (41), now the problem has to be considered self-consistently.

The right-hand boundary condition, Eq. (10), remains unchanged, while the left-hand condition for the relaxed part of the chain now takes the form

$$u_L = (f + ku_d)/(k + K), \quad (42)$$

and Eq. (18) is to be modified correspondingly,

$$w_L = w_R + k/(k + K) + w_d, \quad (43)$$

where $w_d = l/u_c = v\tau/u_c$.

For the sawtooth shape of the substrate force, the solution of Eq. (20) now consists of three linear pieces:

$$p(w) = -\frac{1}{2}(1 + \sqrt{1 + 4A})(w - w_R) \quad (44)$$

for $w_R \leq w \leq w_c = 1$,

$$p(w) = -\frac{1}{2}(\sqrt{1 + 4A} - 1)(w_L - w) \quad (45)$$

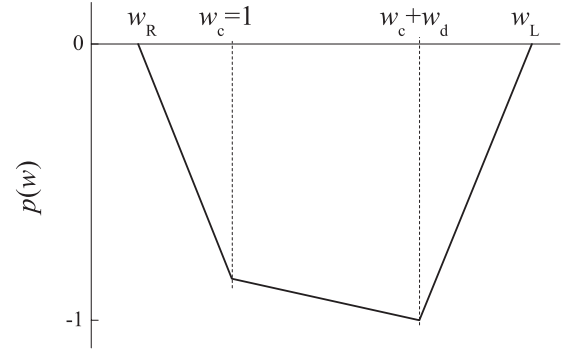


FIG. 6. The function $p(w)$, Eqs. (44)–(46).

for $w_c + w_d \leq w \leq w_L$, and $p(w) = \text{constant} - w$ in between, where $G(w) = 0$,

$$p(w) = 1 - \frac{1}{2}(1 + \sqrt{1 + 4A})(1 - w_R) - w \quad (46)$$

for $w_c + w_d \leq w \leq w_L$, where we made it continuous at the point $w = w_c = 1$. The solution $p(w)$ is shown in Fig. 6. Then, the continuity condition at $w = w_c + w_d$ again gives us an equation for v :

$$\sqrt{1 + 4A} = \frac{q_d + 1}{q_d - 1}, \quad (47)$$

where now

$$q_d = \frac{w_L - 1}{1 + w_d - w_R}. \quad (48)$$

Finally, we can derive the kink shape from the equation $w_y = p(w)$, or $y = \text{constant} + \int dw/p(w)$. The kink moving with the velocity v has different shapes at the right-hand (unrelaxed) side, $x > x_k = vt$,

$$u(x) = u_R + (u_c - u_R)e^{-\beta_R(x-x_k)}, \quad (49)$$

and at the left-hand (relaxed) side, $x < x_k$,

$$u(x) = u_L - (u_L - u_c)e^{\beta_L(x-x_k)}, \quad (50)$$

where

$$\beta_R = (1 + \sqrt{1 + 4A})/2b \quad (51)$$

and

$$\beta_L = (\sqrt{1 + 4A} - 1)/2b. \quad (52)$$

The results, derived in the continuum-limit approximation, can be corrected from discreteness effects when the kink width is not large compared to the lattice spacing. This effect is well known in dislocation theory [8]. A narrow dislocation is not free to move in a crystal lattice but instead it is subjected to a periodic potential, with the period of the lattice and an amplitude known as the Peierls-Nabarro (PN) barrier. The exact calculation of the PN barrier requires the solution of the discrete set of differential equations (5) instead of the continuous partial differential equation (12). However, a good approximation of the discreteness effects can be obtained by substituting the continuum solutions (49) and (50) into the discrete motion equation (5). The discreteness effects imply that a force f_{PN} , adds to the minimal threshold for kink motion,

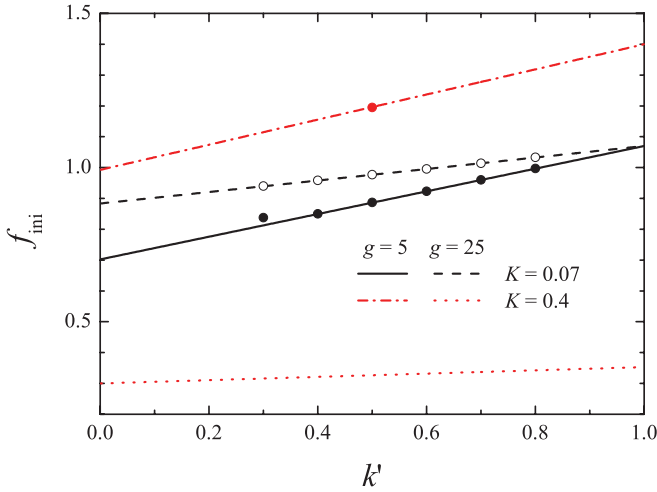


FIG. 7. (Color online) The initial driving force f_{ini} , Eq. (58), as a function of the spring constants k' of the two central contacts for different values of K and g as shown in the legend. The symbols show simulation results.

which for the discrete chain becomes $f_{\text{min}} + f_{\text{PN}}$. As a result the minimal kink velocity becomes nonzero,

$$v_{\text{min}} \approx f_{\text{PN}}/m_k \eta. \quad (53)$$

IV. SIMULATION

The continuum-limit approximation is accurate for the case of strong interaction between the contacts, $g \gg 1$; in the opposite limit one has to use computer simulation. We solved Eq. (5) by the Runge-Kutta method. As the initial state, we took the chain of length N (typically $N = 3 \times 10^3$ or $N = 3 \times 10^4$) with periodic boundary conditions and all contacts relaxed, but the threshold breaking value for two central contacts ($n = 0, 1$) was set to k' , lower than for the other contacts chosen as $k = 1$, as discussed above (Fig. 2). We set $u_c = 1$ for all contacts. Then, as the driving force increases, the two central contacts break first and initiate two solitary waves of subsequent contact breaking which propagate in opposite directions through the chain as schematized in Fig. 2. To speed up the beginning of this process, we used $x_{\text{ini}} > 0$ in Eq. (6).

Typical scenarios are shown in Figs. 3 and 4. The value k' of the lower threshold of the central contacts determines the driving force that initiates the rupture front, and therefore the kink velocity. The lower this threshold, the lower the force for which the motion starts. Figure 7 shows the value of the driving force that initiates the front versus k' .

Let us consider first the case of the simplified sawtooth shape for $F(u)$, Eq. (7). In this case the force that initiates the motion can be calculated exactly.

In the symmetric stationary state just before the beginning of the kinks motion, the equations of motion take the form

$$-g(u_{n+1} + u_{n-1} - 2u_n) + (k + K)u_n = f \quad \text{for } n \geq 2 \quad (54)$$

and

$$-g(u_2 - u_1) + (k' + K)u_1 = f \quad \text{for } n = 1. \quad (55)$$

The general solution of Eq. (54) is $u_n = U + A\rho^{n-1}$ and, to cancel the site-independent parts we have to choose $U = f/(k + K)$. Then Eq. (54) reduces to a quadratic equation for ρ . Only the solution $\rho < 1$ is meaningful to avoid a divergence of u_n so that we get

$$\rho = 1 - \alpha[\sqrt{1 + 2/\alpha} - 1] \quad \text{with } \alpha = (K + k)/(2g). \quad (56)$$

The threshold for the motion is obtained when u_1 reaches the value $u_1 = u_c = 1$. Then Eq. (55) for site $n = 1$ gives an expression for $u_2 = U + A\rho$, so that it determines the amplitude factor A

$$A\rho g = (k' + K + g) - f[1 + g/(K + k)]. \quad (57)$$

Finally Eq. (54), written for site $n = 2$ can be used to extract f , which is the minimal force necessary to initiate the motion as it raises u_1 to the threshold u_c . We get

$$f_{\text{ini}} = \left[g - (k' + K + g) \left(2 - \rho + \frac{k + K}{g} \right) \right] / \left[\rho \left(1 + \frac{g}{K + k} \right) - 3 - \frac{g}{K + k} - \frac{K + k}{g} \right], \quad (58)$$

where ρ is given by Eq. (56).

Figure 7 shows how f_{ini} depends on k' . The theoretical results are well verified by the simulations.

As soon as the kink motion is initiated, the k values of the central contacts are restored to the same value as for other contacts (otherwise these contacts would act as a source for creation of new pairs of kinks). Because the driving force increases with time according to Eq. (6), the kink velocity increases too, as shown in Fig. 3. In order to avoid kink acceleration, we used the following algorithm: as soon as kink motion is initiated at $t = t_b$, we begin to move the substrate in the opposite direction, $v_d > 0 \rightarrow v_b < 0$, so that the driving force linearly decreases with time [see Fig. 8(b)], and the average chain velocity $\langle \dot{x}_i \rangle = N^{-1} \sum_i \dot{x}_i$ decreases as well [Fig. 8(c)] until the motion stops [Fig. 8(a)]. In a single simulation this algorithm allows us to find the dependence of the kink velocity defined as

$$v = n_k^{-1} N (\langle \dot{x}_i \rangle - \bar{v}), \quad (59)$$

where $n_k = 2$ is the number of moving kinks in the chain and $\bar{v} = \dot{u}_{L,R} = v_b K/(k + K)$ is the background velocity on the driving force f . These dependences are presented in Fig. 9 for two values of the coupling constant g . They are in good agreement with the predictions of Eqs. (33) and (37).

However, in the discrete lattice, contrary to the continuum-limit approximation, the velocity of the kink oscillates during the motion as demonstrated in Fig. 8(d). This is the consequence of the periodic PN potential. The stronger the elastic interaction between the contacts, the larger the kink width [compare Figs. 4(a) and 4(b)], which results in smaller kink oscillations [compare Figs. 9(a) and 9(b)], which also leads to a smaller minimal kink velocity. Simulations for different delay times τ show that this parameter has only a marginal effect on the curves $v(f)$.

In the general case, the λ contacts are characterized by a smooth dependence $F(u)$ which follows from the

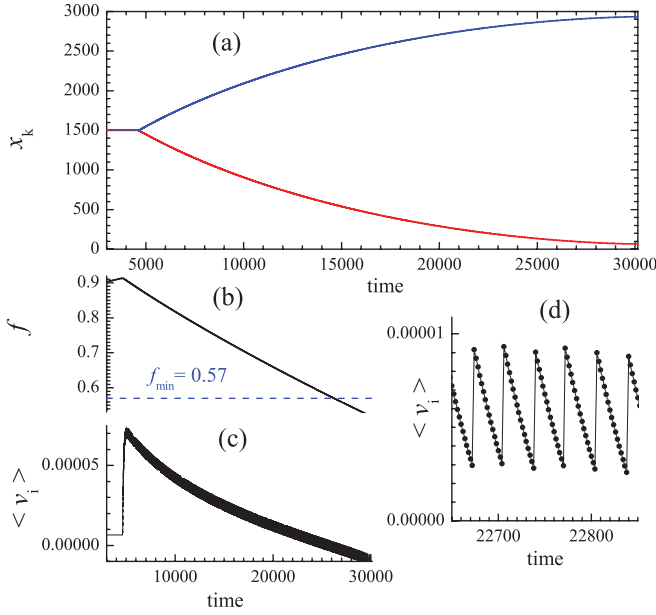


FIG. 8. (Color online) Evolution of the chain of $N = 3000$ contacts. The nearest neighboring contacts interact elastically with the constant $g = 25$; the interaction with the substrate is modeled by the sawtooth function (7) with $k = 1$ and $u_c = 1$. All contacts are driven through the springs of the elastic constant $K = 0.07$, their ends moving with the velocity $v_d = 10^{-4}$. The motion is overdamped ($m = 1$, $\eta = 100$). To initiate the breaking, two central contacts interact with the substrate with smaller spring constants, $k' = 0.5$. To speed up the simulation, we used $x_{\text{ini}} = 13.5$. When the kinks motion begins at $t = t_b$, the elastic constants of the central contacts recover their values to $k = 1$, and the driving velocity changes its sign, $v_d \rightarrow v_b = -2 \times 10^{-4}$. (a) shows the kinks centers (defined as places where the atomic velocity is maximal), (b) shows the driving force, Eq. (6), and (c) shows the average chain velocity $\langle \dot{x}_i \rangle = N^{-1} \sum_i \dot{x}_i$. What appears as a thick line actually corresponds to the velocity oscillations, which are not resolved due to the large time range covered by this figure. Panel (d) shows the details in a smaller time domain. (d) demonstrates the oscillation of the velocity due to PN barriers.

master-equation approach, instead of the sawtooth shape. An elastic instability, i.e., a stick-slip behavior of the λ contacts occurs only if $K \leq -dF(u)/du|_{u=u_c}$. Figure 10 shows the effect of various distributions $P_c(u)$ of the breaking threshold of the individual contacts. When this distribution reduces to a Dirac delta function, $F(u)$ given by the master equation is simply the sawtooth function assumed for the above simulation results. When the distribution gets broader, the function $F(u)$ becomes smooth. The equation $K + dF(u)/du = 0$ defines the threshold displacement u_{th} and the force $F_{\text{th}} = F(u_{\text{th}})$, for which a λ contact breaks. The effect of a smooth function $F(u)$ over the force-velocity curves for the kinks $v(f)$ is shown in Fig. 11. The basic effect of a smoother function $F(u)$ is to decrease the minimal velocity (53) of the rupture fronts.

V. DISCUSSION

The FK-ME model used here is quite close to the well-known one-dimensional (1D) Burridge-Knopoff model of earthquakes with a velocity-weakening friction law [9]. The

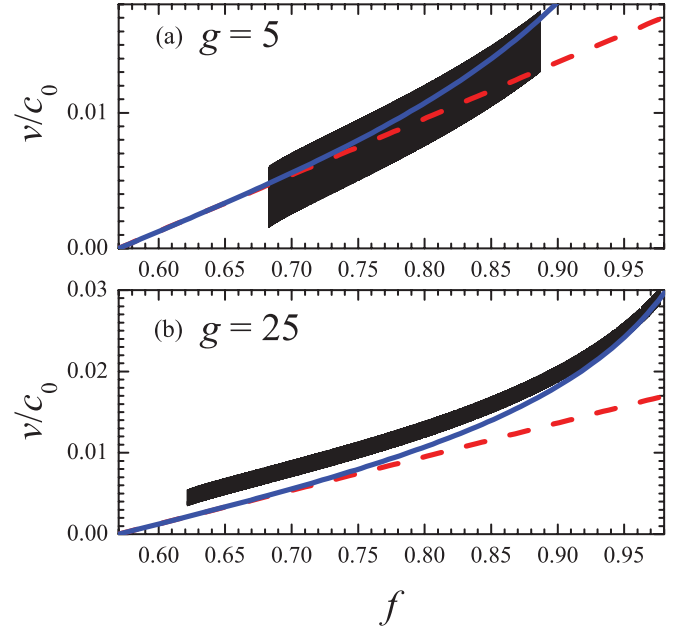


FIG. 9. (Color online) Kink velocity (normalized on the sound velocity c_0) versus the driving force for (a) $g = 5$ ($x_{\text{ini}} = 12.5$, $v_b = -4 \times 10^{-6}$) and (b) $g = 25$ ($x_{\text{ini}} = 13.5$, $v_b = -2 \times 10^{-5}$); $N = 3 \times 10^4$, other parameters as in Fig. 8. The interaction with the substrate is modeled by the sawtooth function (7) with $k = 1$ and $u_c = 1$. Blue solid and red dashed lines correspond to Eqs. (33) and (37). What appears as thick lines actually corresponds to velocity oscillations [see Fig. 8(d)], which are not resolved due to the large force range covered by the present figure.

difference lies in the substrate friction force F . Instead of the friction law of a single contact or a phenomenological velocity-dependent function, we incorporate the collective effects which occur in a set of contacts that are interconnected by a bulk material that is rigid on the short spatial scale λ_c . This allows much richer behaviors for $F(u)$, which can, for instance, include temperature effects and the aging properties of the collective contacts. Applying the methods developed for the standard FK model to this system allows us to make analytical predictions for the rupture fronts, which are analogous to the solitons of the FK model in the presence of discreteness effects. There are nevertheless significant differences. In the FK model, which corresponds to $\mathcal{F}(u) \propto \sin u$, the effective potential has degenerate minima. In the continuum limit this implies that solitons can move in the positive or negative direction even at vanishingly small velocities, without a driving force. The FK-ME model is different because $\mathcal{F}(u) = F(u) + Ku - f$ [see Eq. (9)] is constructed from a function $F(u)$ which is always positive. This implies that kinks/antikinks can only move from relaxed to unrelaxed regions and that a nonzero force f_{min} is required to have two degenerate minima in the effective potential of the model (Fig. 5), and allow a kink motion even in the continuum limit. In the presence of discreteness the minimal force is increased by the amount f_{PN} required to overcome the PN barrier, and this also implies a nonzero minimal velocity for the kinks. The importance of this minimal force, and velocity, is an important result of this study because it shows how a model that stays fairly simple, but incorporates the complexities arising from

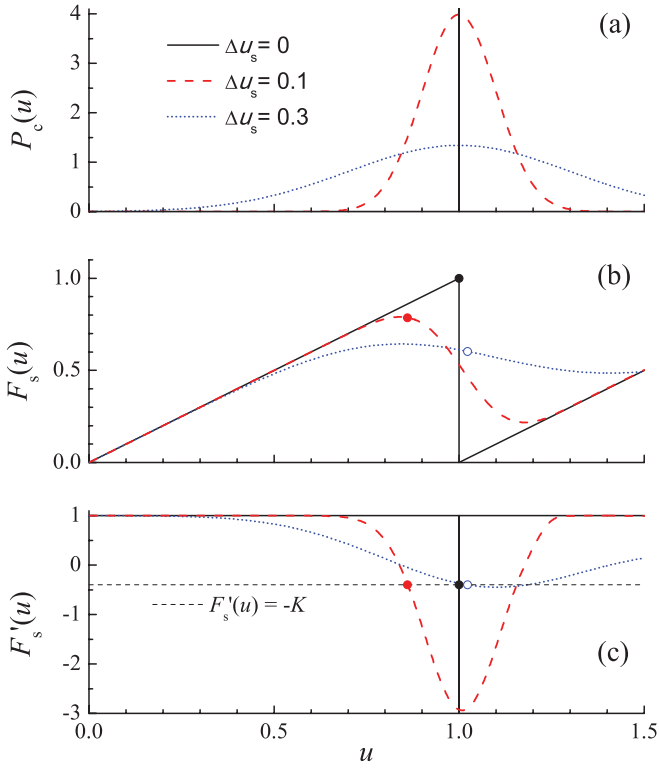


FIG. 10. (Color online) (a) Gaussian distribution of static thresholds $P_c(u)$, (b) the function $F(u)$ obtained from solution of the master equation, and (c) the function $F'(u)$ for $u_s = 1$ and three values of the dispersion $\Delta u_s = 0, 0.1$, and 0.3 . Points indicate displacements where the elastic instability occurs.

the collective behavior of individual contacts, can exhibit a rupture mode reminiscent of the “slow rupture mode” observed experimentally [3]. Moreover, the analysis in terms of a variant of the FK model allows us to propose some analytical understanding of these slow rupture modes.

In spite of the differences between the FK-ME model discussed here and the standard FK model, the analogies could perhaps be exploited to proceed further:

(1) The driven FK model exhibits hysteresis when the force increases and then decreases [8,10]. The same was observed in large-scale crack simulation [11], and thus could be observed in friction too.

(2) The effects of nonzero temperature may be considered as well. One may predict that at $T > 0$ the sliding kinks will experience an additional damping, while the immobile (below threshold) kinks will slowly move (creep) due to thermally activated jumps.

(3) As shown in Refs. [8,12], in the FK model fast driven kinks begin to oscillate due to excitation of a shape mode, and then, with a further increase of driving, the kinks are destroyed. This effect is similar to what is observed in fracture mechanics, where cracks begin to oscillate and then branch [13].

(4) One may suppose that the damping coefficient η in the equation of motion (5) depends on the kink velocity, so that $\eta(v)$. In fracture mechanics, this coefficient defines the rate at which the energy is removed from the crack edge, thus it plays a crucial role.

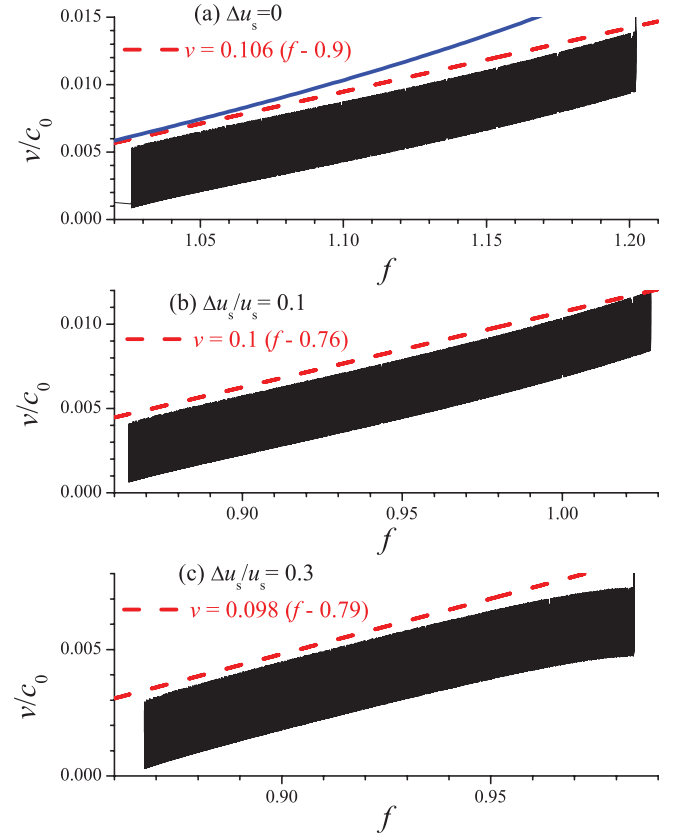


FIG. 11. (Color online) Kink velocity (normalized on the sound velocity c_0) versus the driving force for $N = 30\,000$, $\eta = 100$, $g = 5$, $K = 0.4$, $v_d = 2 \times 10^{-5}$ and (a) $\Delta u_s = 0$ [$x_{\text{ini}} = 2.9$, $v_b = -8 \times 10^{-7}$; blue solid and red dashed lines correspond to Eqs. (33) and (37), correspondingly], (b) $\Delta u_s = 0.1$ ($x_{\text{ini}} = 2.4$, $v_b = -6 \times 10^{-7}$), and (c) $\Delta u_s = 0.3$ ($x_{\text{ini}} = 2.2$, $v_b = -4 \times 10^{-7}$). Red dashed lines in (b) and (c) show just fits. The interaction with the substrate uses the function $F(u)$ deduced from the solution of the master equation, plotted in Fig. 10. What appears as black thick lines actually corresponds to velocity oscillations, which are not resolved due to the large force range covered by the present figure.

These points open many possibilities for the development of this work, but some of its limitations should, however, not be ignored and will require further studies.

The possibilities for a quantitative comparison with experiments is limited because the model has been simplified to allow analytical investigations: (i) all λ contacts are identical and (ii) the driving force is identical for all contacts, in contrast with most of the experiments where it is applied on one end of the system, and the pressure is generally not uniform. Contrary to earlier studies based on numerical approaches [14–16], the present study is mostly relevant to investigate the properties of the rupture fronts once they have been created, while experimental data also depend on the conditions for the creation of the fronts. Nevertheless, our approach gives a possible answer to an intriguing question about the slow rupture front observed at experiments [3] and in simulation [14,15]. Recall that a typical crack speed in bulk is of order $(0.2\text{--}0.6)c_0$ [13], while the slow detachment front moves with a velocity $\sim 0.02c_0$. If the self-healing crack in the frictional interface corresponds to a solitary wave, than

its minimal velocity is determined by the amplitude of the PN barrier, Eq. (53). Estimation predicts that $g \gg 1$ for a realistic case of contact of rough surfaces [6], which leads to exponentially small values of v_{\min} . In this case the kink velocity will be determined by the shear stress at the interface and the damping coefficient η that describes the energy loss in the interface, which flows to the bulk and is dissipated by heat.

The main difficulty resides in the decomposition of the friction problem into a study of the λ contact and then the cooperative behavior of these λ contacts in the presence of the elasticity of the bulk. A λ contact describes a collection of asperities. The master equation formalism, which determines the statistical behavior of the asperities attached to a rigid substrate is well defined and can be applied in a systematic way. The determination of the effective elasticity k_λ for a λ contact is more difficult because it can only be rigorously obtained by a treatment of a three-dimensional elastic problem. Presently the separation that we introduced between the material belonging to the λ contact and the bulk is not defined in a systematic way. A more rigorous treatment of the boundary conditions between these elements, in the spirit of what is done in finite elements methods of continuum mechanics, should clarify this point.

Throughout the paper we assumed that all λ contacts are characterized by the same $F(u)$ dependence and thus have the same threshold value. As the distribution of their thresholds is narrower than the distribution of thresholds of single asperities by a factor $\sqrt{N_\lambda}$, this is a good approximation if the number of original contacts within a single λ contact, $N_\lambda = (\lambda_c/a)^2$, is large. However, even a narrow distribution of thresholds will have a qualitative effect because rupture fronts may stop when they meet λ contacts with a threshold above the driving force. When the interface is disordered, the avalanches will have finite lengths and may become short for forces near f_{ini} , for which the rupture fronts propagate at the minimal velocity.

In the present work we also ignored the existence of defects always present in real materials. The role of disorder and

defects in driven systems is a rather complicated problem which attracted much attention. On one hand, defects may stimulate kinks creation, but on the other hand, kinks propagation may be slowed down up to its complete arrest due to pinning on the defects. For example, the slowing down of the 1D crack propagating through a two-dimensional (2D) system with quenched randomly distributed defects was considered in Ref. [17].

Moreover in the simulation of Sec. IV we started from a well-defined initial configuration, where all contacts are relaxed except the one or two where the kink's motion is initiated. If one starts from a random initial configuration, we expect that kinks will emerge at random places, so that several kinks may propagate through the system simultaneously, as was observed in simulation of the Burridge-Knopoff model [18].

Another obvious generalization is to extend the 1D model to 2D. We do not expect this to introduce qualitative changes. In the 2D interface, the interaction in the shear direction is stronger than in the transverse direction [6], thus we expect that an avalanche should take an oval shape elongated in the driving direction, but preserve its main features. This could nevertheless affect the trapping of the rupture fronts by inhomogeneities and thus qualitatively affect the frictional properties of a real system.

The work that we presented here is only a first attempt to describe the propagation of rupture fronts in friction while taking into account the properties of the interface at different scales and the elastic properties of the sliding block. Obviously there is much more to do in this direction, but the possibility to cast the problem in the framework of the well-known FK model allows a first-level analysis which brings useful ideas for further extensions.

ACKNOWLEDGMENTS

This work was supported by CNRS-Ukraine PICS Grant No. 5421.

-
- [1] O. M. Braun and M. Peyrard, *Phys. Rev. Lett.* **100**, 125501 (2008).
 - [2] O. M. Braun and M. Peyrard, *Phys. Rev. E* **82**, 036117 (2010).
 - [3] O. Ben-David, G. Cohen, and J. Fineberg, *Science* **330**, 211 (2010).
 - [4] A. Schallamch, *Wear* **17**, 301 (1971).
 - [5] C. Caroli and Ph. Nozieres, *Eur. Phys. J. B* **4**, 233 (1998).
 - [6] O. M. Braun and D. V. Stryzheus (unpublished); O. M. Braun, M. Peyrard, D. V. Stryzheus, and E. Tosatti, *Tribol. Lett. (to be published)*, doi:10.1007/s11249-012-9913-z.
 - [7] L. D. Landau and E. M. Lifshitz, *Theory of Elasticity. Course of Theoretical Physics* (Pergamon Press, New York, 1986), Vol. 7.
 - [8] O. M. Braun and Yu. S. Kivshar, *The Frenkel-Kontorova Model: Concepts, Methods, and Applications* (Springer-Verlag, Berlin, 2004).
 - [9] R. Burridge and L. Knopoff, *Bull. Seismol. Soc. Am.* **57**, 341 (1967).
 - [10] O. M. Braun, A. R. Bishop, and J. Röder, *Phys. Rev. Lett.* **79**, 3692 (1997).
 - [11] D. Holland and M. Marder, *Phys. Rev. Lett.* **80**, 746 (1998).
 - [12] O. M. Braun, B. Hu, and A. Zeltser, *Phys. Rev. E* **62**, 4235 (2000).
 - [13] J. Fineberg and M. Marder, *Phys. Rep.* **313**, 1 (1999).
 - [14] O. M. Braun, I. Barel, and M. Urbakh, *Phys. Rev. Lett.* **103**, 194301 (2009).
 - [15] S. M. Rubinstein, I. Barel, Z. Reches, O. M. Braun, M. Urbakh, and J. Fineberg, *Pure Appl. Geophys.* **168**, 2151 (2011).
 - [16] J. Tromborg, J. Scheibert, D. S. Amundsen, K. Thøgersen, and A. N. Malthe-Sørensen, *Phys. Rev. Lett.* **107**, 074301 (2011).
 - [17] J. Kierfeld and V. M. Vinokur, *Phys. Rev. Lett.* **96**, 175502 (2006).
 - [18] J. Schmittbuhl, J.-P. Vilotte, and S. Roux, *Europhys. Lett.* **21**, 375 (1993).